MNRAS **000**, 1–8 (2019) Preprint 27 March 2019 Compiled using MNRAS LATEX style file v3.0

The Globular Cluster System of the Auriga Simulations

Timo L. R. Halbesma[1]★, Robert J. J. Grand[1], Volker Springel[1], Facundo A. Gómez[2,3], Federico Marinacci[4,5], Rüdiger Pakmor[1], Wilma Trick[1], Philipp Busch[1], Simon D. M. White[1]

[1] *Max-Planck-Institut für Astrophysik, Karl-Schwarzschild-Str. 1, 85741 Garching, Germany*
[2] *Instituto de Investigación Multidisciplinar en Ciencia yTecnología, Universidad de La Serena, Raúl Bitrán 1305, La Serena, Chile*
[3] *Departamento de Física y Astronomía, Universidad de La Serena, Av. Juan Cisternas 1200 N, La Serena, Chile*
[4] *Department of Physics, Kavli Institute for Astrophysics and Space Research, MIT, Cambridge, MA 02139, USA*
[5] *Harvard-Smithsonian Center for Astrophysics, 60 Garden Street, Cambridge, MA 02138, USA*

Accepted XXX. Received YYY; in original form ZZZ

ABSTRACT

Rob Grand: 'for many Auriga papers Carlos Frenk and Adrian Jenkins are offered co-authorship. Perhaps you could ask Simon about this.'

We investigate whether the galaxy formation model used for the Auriga simulations can produce a realistic globular cluster population at redshift zero. We compare properties of the simulated star particles in the Auriga haloes with catalogues of observations of the Milky Way globular cluster population available in the literature. We find that the Auriga simulations do produce sufficient mass at radii and metallicities that are typical for the MW GCS, although we observe a varying mass-excess for the different $R_{\rm GC}$-[Fe/H] bins. This implies different values for the combined product of the bound cluster formation efficiency and the globular cluster disruption rate. We investigate wether these differences could result from formation insitu vs. accreted star particles. We find ... TODO. Furthermore we test whether any of the Auriga galaxies has a metallicity and radial distribution that is consistent with the MW (M31) GCS. For all of the Auriga haloes we reject the null hypothesis that the simulated and observed metallicities are drawn from the same distribution at the 99.99% confidence level, for the GCS of the Milky Way as well as that of the Andromeda galaxy. The same holds true for the distribution of galactocentric radius.

Key words: methods: numerical – galaxies: formation – galaxies: star clusters: general.

1 INTRODUCTION

Globular clusters (GC)s are omnipresent, bright, old, and amongst the simplest stellar configurations in the Universe. Their visbility and ubiquity make it possible to obtain integrated GC quantities within the Virgo Supercluster. Moreover, GCs inherit characteristics from their natal gas and GC systems show correlations with properties of (the field stars in) their host galaxies. The old ages are consistent with formation before, during, or shortly after the initial collapse of the proto-galaxy and GCs have been present within galaxies for nearly a Hubble time. In theory, all of these characteristics make GC systems excellent tracers of the formation and evolution of their parent galaxies, if the formation of GCs themselves is well-understood.

Most galaxies host GC systems with a bimodal colour distribution, indicative of a bimodal metallicity distribution. The Milky Way (MW) GC system (GCS) can be split up in a metal-rich (red) and metal-poor (blue) subpopulation divided at [Fe/H] = −1 (e.g. Harris 2001), although slightly different values can also be found in the literature. The two subpopulations are believed to be associated to the galactic disk, respectively the stellar halo (e.g. Zinn 1985). The latter is supported by observed similarities between the spatial distribution and chemical signature of the 'blue' GCs show and stars in the stellar halo (Helmi 2008). Moreover, relative age-estimates indicate that the metal-poor subpopulation may be 1.5 Gyr younger than the metal-rich counterpart (De Angeli et al. 2005).

Several formation scenarios could explain the observed bimodality, see Brodie & Strader (2006) for a review of extragalactic GCs and galaxy formation. The authors argue that the observed metal-rich and metal-poor

- Special conditions in early Universe?
- Formation in collapsing proto-galaxies (in-situ-ish?)

★ E-mail: Halbesma@MPA-Garching.MPG.DE

- Formation as a result of (wet) mergers?
- Formation in satellites that are later accreted?
- No special conditions at high z, but connection between low-z YMC- and high-z GC-formation where differences could result from Hubble time of evolution?
- This means that in order to test formation models against observations, one not only needs needs to model GC formation, but also include the full evolution over their lifetime in a cosmological tidal field.

Paragraph: ingredients for numerical studies

- High resolution in the ISM
- Full cosmological evolution

Paragraph: narrow down to this work

- The star formation model implemented in the Auriga simulations is capable of producing a suite/population of realistic Milky Way-like galaxies at redshift zero.
- Therefore the question naturally arises whether or not the Auriga simulations are also capable of faithfully producing a globular cluster population as observed in the Milky Way (or Andromeda).
- Globular cluster formation in cosmological zoom simulations is very interesting for two reasons. First of all, extragalactic observations typically show the integrated properties of globular clusters rather than that of the individual stars within the clusters. Moreover, the typical mass scale of globular clusters is comparable to the numerical (mass) resolution of cosmological zoom simulations. The detailed small scale physics that is at play for real world globular clusters appears in observations as the combined effect of the 10^{3-6} $M_\odot$, compared to a mass resolution of 10^{3-5} $M_\odot$for the Auriga simulations. Globular clusters can therefore serve as an ultimate test to the star formation model that is implemented in the numerical simulations. Secondly, cosmological zoom simulations provide an accurate recording of the full and detailed merger history of the simulated galaxy. This is important because theoretical paradigms for globular cluster formation in the literature know two distinct classes of GCs that are separated by their exact formation sites: an in-situ versus an accreted population. Cosmological zoom simulations uniquely allow for an investigation into globular cluster formation with particular focus on the in-situ and accreted populations.

Paragraph: Paper outline

We summarise the relevant characteristics of the Auriga simulations in section 2, followed by a summary of the observations of the Milky Way (MW) globular cluster system (GCS) in section 3 that we use to compare our simulations to in section 4. We discuss our findings in section 5 to come to our conclusions in section 6.

2 THE AURIGA SIMULATIONS

We use the Auriga simulations (Grand et al. 2017, hereafter G17), a suite of high-resolution cosmological zoom simulations of Milky Way-mass selected initial conditions. The simulations are performed with the state-of-the art code AREPO (Springel 2010; Pakmor et al. 2016), that solves the magnetohydrodynamical equations on a moving mesh, and an elaborate galaxy formation model that produces realistic spiral galaxies at redshift $z = 0$.

The interstellar medium is modelled using a sub-grid approach which implements the physical processes most relevant to galaxy formation and evolution. This model was tailored to the AREPO code and calibrated to reproduce key observables of galaxies, such as the history of the cosmic star formation rate density, the stellar mass to halo mass relation, and galaxy luminosity functions.

The sub-grid includes primordial and metal-line cooling with self-shielding corrections. Reionization is completed at redshift six by a time-varying spatially uniform UV background (Faucher-Giguère et al. 2009; Vogelsberger et al. 2013) The interstellar medium is described by an equation of state for a two-phase medium in pressure equilibrium (Springel & Hernquist 2003) with stochastic star formation in thermally unstable gas with a density threshold of $n = 0.13\mathrm{cm}^{-3}$, and consecutive stellar evolution is accounted for. Stars provide feedback by stellar winds (Marinacci et al. 2014; Grand et al. 2017), and further enrich the ISM with metals from SNIa, SNII, and AGB stars (Vogelsberger et al. 2013). The formation of black holes is modelled which results in feedback from active galactic nuclei (Springel et al. 2005; Marinacci et al. 2014; Grand et al. 2017). Finally, the simulations follow the evolution of a magnetic field of 10^{-14} (comoving) G seeded at $z = 127$ (Pakmor & Springel 2013; Pakmor et al. 2014). See G17 for further details of the numerical setup as well as the galaxy formation model.

The Auriga suite has a fiducial resolution level L4, accompanied by the lower (higher) level L5 (L3) that is available for selected initial condition runs. The baryonic mass resolution in order of increasing level is $m_b = [4 \times 10^5, 5 \times 10^4, 6 \times 10^3]$ $M_\odot$ with gravitational softening of collissionless particles $\epsilon = [738, 369, 184]$ pc.

3 OBSERVATIONAL DATA

We summarise relevant observations of the globular cluster system of the Milky Way in Sec. 3.1, and of Andromeda (M31) in Sec. 3.2.

3.1 Milky Way

Harris (1996, 2010 edition; hereafter H96e10) provides a catalogue[1] of the Milky Way globular cluster system that contains properties of 157 GCs. The authors initially estimated the size of the MW GCS to be 180 ± 10, thus, their catalogue to be ~85% complete. However, an additional 59 GCs have since been discovered by various authors. The total confirmed number of GCs in the MW adds up to 216 with new estimates now anticipating an additional thirty GCs yet to be discovered (e.g. Ryu & Lee 2018, and references therein).

Bica et al. (2019) communicate the latest efforts to aggregate the available data, presented in their CatClu catalog. Amongst 10978 star clusters and alike objects in the Milky Way, the catalog contains 200 GCs and 94 GC candidates. The CatClu catalog contains reference papers, positions, distances, and total absolute V magnitude. Therefore we rely on the H96e10 dataset for all other quantities, but we caution that the Harris catalogue is now believed to be (only) 53-72% complete.

Specifically, the relevant data fields that we use from H96e10 are the metallicity [Fe/H], the Galactic distance components X, Y, and Z (in kpc)[2], and absolute magnitude in the V-band M_V. We use the latter to calculate mass-estimates by assuming $M_{V,\odot} = 4.83$

[1] See https://www.physics.mcmaster.ca/Fac_Harris/mwgc.dat

[2] In a Sun-centered coordinate system: X points toward Galactic center, Y in direction of Galactic rotation, and Z toward the North Galactic Pole. We calculate the galactocentric radius $R_{\mathrm{GC}} = \sqrt{(X - R_\odot)^2 + Y^2 + Z^2}$, assuming the solar radius $R_\odot = 8$ kpc.

and a mass to light ratio $M/L_V = 1.7$ M/L$_\odot$, the mean for MW clusters (McLaughlin & van der Marel 2005).

3.1.1 *Age estimates*

We supplement H96e10 with age-estimates from isochrone fits to stars near the main-sequence turnoff in 55 GCs (VandenBerg et al. 2013, hereafter V13). The mean value of the age-estimates in this data set is 11.9 ± 0.1 Gyr and the dispersion is 0.8 Gyr. Furthermore, only one of the 55 GC age-estimates is below 10 Gyr.

3.2 Andromeda

The fifth revision of the revised bologna catalogue (RBC 5, last updated August, 2012) is the latest edition of three decades of systematically collecting integrated properties of the globular cluster system of the Andromeda galaxy (Galleti et al. 2004, and references therein). One contribution to RBC 5 is the work by Caldwell et al. (2011, hereafter C11), subsequently updated by Caldwell & Romanowsky (2016, hereafter CR16).

C11 and CR16 present a uniform set of spectroscopic observations calibrated on the Milky Way GCS of the inner 1.6° (~ 21) kpc that is believed to be 94% complete. GCs in the outer stellar halo, up to $R_{\rm proj} \sim 150$ kpc, are observed in the Pan-Andromeda Archaeological Survey (PAndAS, Huxor et al. 2014, hereafter H14), but see also Veljanoski et al. (2014) and Mackey et al. (2019). H14 presents the discovery of 59 new GCs and publishes updates to RBC 5. The work of H14 is incorporated in the latest public release[3] of the C11 dataset, further revised by CR16. It seems that CR16 is the most recent aggregated dataset of M31's GCS that contains properties of interest for our study as it contains GCs in the inner region and in the outer halo. The relevant fields in the CR16 dataset that we use are the age, metallicity, and the mass-estimate[4].

3.2.1 *Age estimates*

For M31 we find an age distribution with a mean value of 11.0±0.2 Gyr and a dispersion of 2.2 Gyr. Furthermore, 24 GCs have age-estimates below 10 Gyr, and the minimum age is 4.8 Gyr.

We present a mass-weighted histogram of the age-estimates of the 55 MW GCs in V13 and 85 GCs in M31 for which age-estimates are available in CR16, see Figure 1.

3.3 Total GC mass in metallicity-radial space

We show the two-dimensional mass-weighted metallicity-radial distribution of the MW (M31) GCS in the top (bottom) panel of Figure 2. Both quantities are readily available in H96e10, but the galactocentric radius of GCs in M31 is not available in CR16. Therefore we follow Wang et al. (2019, Sec. 4.1) to calculate the projected radius $R_{\rm proj}$ from the observed positions, adopting M31's central position from the NASA Extragalactic Database[5] $(\alpha_0, \delta_0) = (0^{\rm h}42^{\rm m}44.35^{\rm s}, +41°16'08.63")$ and distance $D_{\rm M31} = 778$ kpc (McConnachie et al. 2005; Conn et al. 2012). We calculate $R_{\rm GC}$ as 'average deprojected distance' $R_{\rm GC} = R_{\rm proj} \times (4/\pi)$. We compare these observations to the Auriga simulations later on in Sec. 5.3,

[3] Last revised 23 Sep 2015, see https://www.cfa.harvard.edu/oir/eg/m31clusters/M31_Hectospec.html
[4] The authors assumed $M/L_V = 2$ independent of [Fe/H]
[5] https://ned.ipac.caltech.edu/

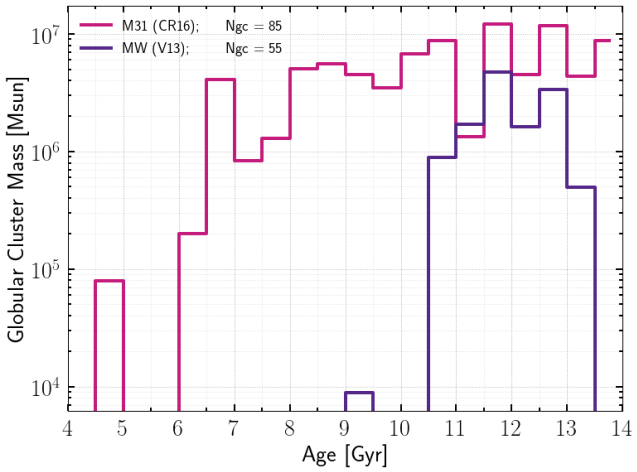

Figure 1. Mass-weighted age distribution of 55 GCs in the MW (data from VandenBerg et al. 2013) and 85 GCs in M31 (data from Caldwell & Romanowsky 2016).

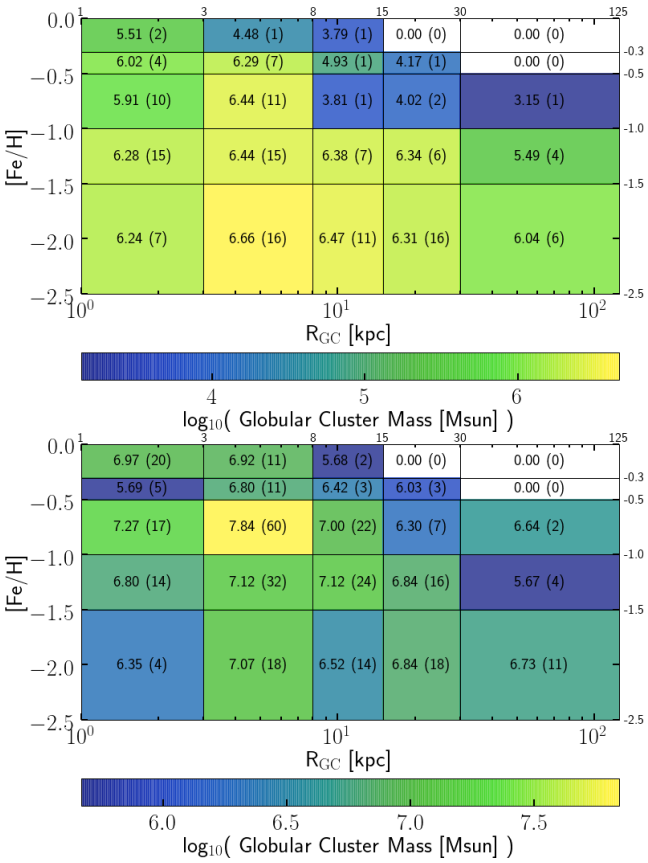

Figure 2. *Top*: Mass-weighted $R_{\rm GC}$-[Fe/H] distribution of 151 GCs in the MW (data from Harris 1996, 2010 ed.), which is 98.19 % of the total MW GCS mass in the Harris catalog. *Bottom*: Same for M31, showing 366 GCs and 88.38 % of the total mass in CR16 (data from Caldwell & Romanowsky 2016). Note that the range of the colourmap differs in both figures.

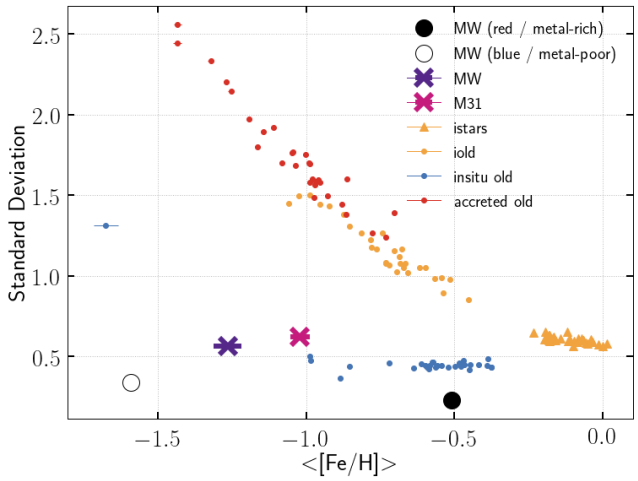

Figure 3. Mean and standard deviation of the metallicity distribution of star particles in each of the thirty Auriga L4 haloes. Orange dots show the subset of old star particles, and blue (red) dots show the old insitu (accreted) component. These Auriga subsets can be compared to the MW (M31) GCS shown in purple (magenta), and to the metal-rich (metal-poor) component of the MW GCS indicated by the black solid (open) dots (values from Ashman & Zepf 1998, p. 38).

4 RESULTS

We define GC candidates in the Auriga simulations as all star particles older than 10 Gyr based on the MW GCS age distribution (Figure 1), and following Renaud et al. (2017).

Trough out the analysis we mainly use three subsets of star particles, the *old stars* (age > 10 Gyr, or GC candidates), the *old in-situ* stars (defined as those bound to the most-massive halo/subhalo in the first snapshot that the particle was recorded), and the *old accreted* star particles (i.e. those that have formed ex-situ and are bound to the most-massive halo/subhalo at $z = 0$). In addition, we include *all stars* (no selection criterion) to examine the result of (not) applying an age cut to our selection functions.

We consider the metallicity distribution in Sec. 4.1 the distribution of galactocentric radii in Sec. 4.2, and the combination of both in Sec. 4.3.

4.1 Metallicity distribution

We investigate whether the star formation model implemented in the Auriga simulations is capable of i) producing a metallicity distribution that is consistent with the GCS observed in the MW (M31), and ii) generating sufficient mass over the domain of the observations.

Figure 3 shows the mean and standard deviation of the [Fe/H] distribution of star particles in all Auriga L4 simulations. The mean metallicity of old star particles lies in the range −1.0 to −0.5 and the dispersion increases with decreasing metallicity. For comparison, the mean of all star particles populates the range −0.25 to 0 with a near-constant dispersion a bit above 0.5. Old accreted stars in the Auriga haloes reach mean metallicities between −1.5 and −1.0, which is considerably lower than the old- and old insitu populations. Most Auriga L4 haloes have old insitu populations with mean metallicities around −0.5. The old accreted populations follow the trent of increasing dispersion with decreasing mean metallicity, but notably the old insitu populations all have a constant dispersion of roughly 0.45. We show the values calculated using all MW (M31) GCs in purple (magenta), and literature values of the metal-rich (metal-poor) component of the MW GCS as black solid (open) dots. We further discuss our comparison between the simulations and the observations in Sec. 5.1

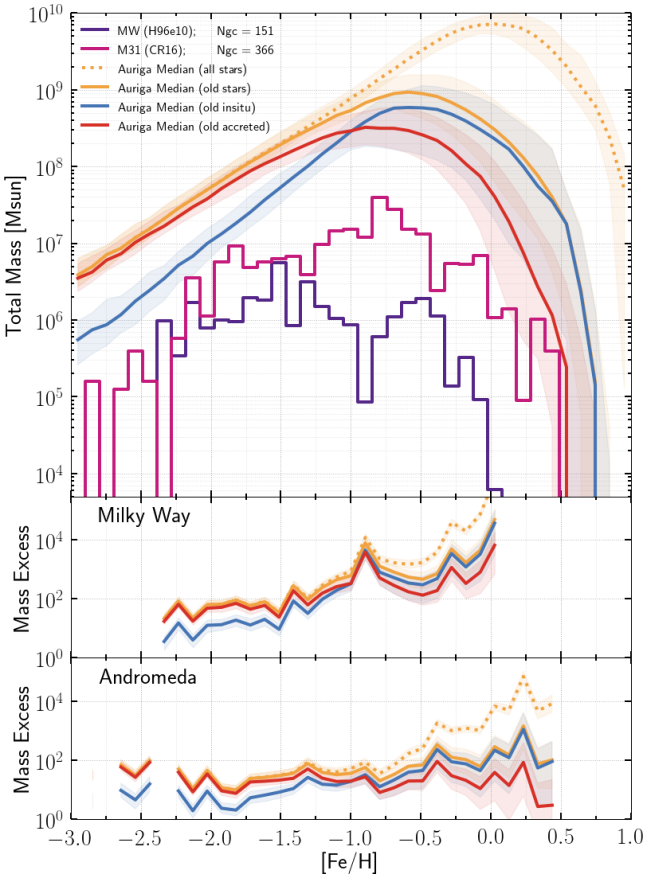

Figure 4. Mass-weighted metallicity distribution of star particles in the Auriga simulations. We show the median value of all Auriga haloes for all stars (orange dotted) and globular cluster candidates (i.e. stars with age > 10 Gyr; orange solid). The latter sub set is further split up between stars that formed in-situ (blue solid), and those that were accreted (red solid). Shaded regions indicate the 1σ interval. The MW (M31) GCS is shown in purple (magenta). The middle (bottom) panel shows the ratio of the simulated mass to the mass in the MW (M31) GCS.

Figure 4 shows the mass-weighted metallicity distribution of the Auriga L4 haloes. Lines show the median value and the shaded regions indicate the 1σ interval around it (i.e. scatter between runs with different initial conditions which thus have unique merger histories). We notice again that the peak metallicity shifts down from 0 to −0.5 for old stars (orange solid) compared to all stars (orange dotted) while the mass at the peak lowers by roughly one dex. The mass budget of the old stars is dominated by the old insitu population (blue solid) below [Fe/H]=−1, and by the old accreted stars (red solid) above this value. We show the MW (M31) GCS in purple (magenta) and we show the ratio of the simulated to the observed profiles in the middle (bottom) panel. This mass excess can be thought of as a combination of the bound cluster formation efficiency and disruptive processes, further discussed in Sec. 5.5.

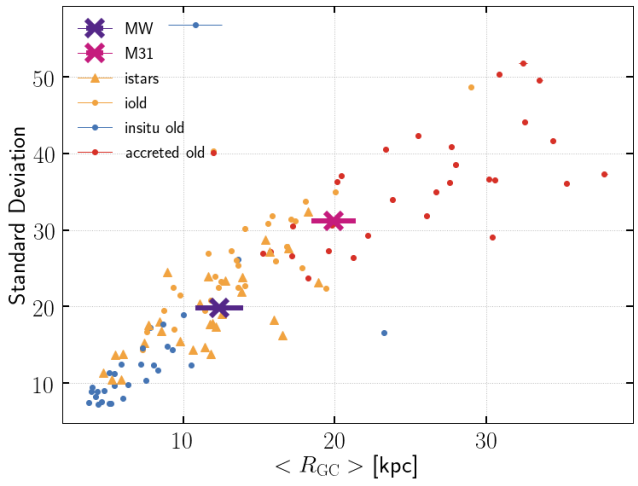

Figure 5. Mean and standard deviation of the radial distribution of star particles in each of the thirty Auriga L4 haloes compared to the MW (M31) GCS shown in purple (magenta).

4.2 Radial distribution

Figure 5 shows the mean and standard deviation of the radial distribution of star particles in all Auriga L4 simulations. We notice that the old insitu populations are much more centrally distributed, whereas the old accreted component has a larger radial extent. Moreover, the dispersion increases with increasing mean value of the radial distribution.

Figure 6 shows the mass-weighted radial distribution of the Auriga L4 haloes. We notice a subtle peak around 10 kpc for all star particles that is not present for the old star particles, indicating that the stellar disc is no longer present when applying the latter selection criterion. Furtermore, we find that the dominant contribution to the total mass in old stars changes from those formed insitu to the accreted population around 10 kpc. We further discuss our comparison between the simulations and the observations in Sec. 5.2.

4.3 Total mass in metallicity-radial space

We investigate whether the Auriga simulations still produce sufficient mass in old star particles to be consistent with the MW (M31) GCS when two-dimensionally binned in both [Fe/H] and R_{GC}. We sum the total simulated mass in each bin and then divide it by the total mass in the MW (M31) GCS. We show this mass excess in Figure **??**, respectively Figure **??**

5 DISCUSSION

5.1 Metallicity distribution

Ashman & Zepf (1998, p. 234) and Harris (2001, p. 38) describe the bimodal [Fe/H] distribution of the MW GCS. The latter fits a double Gaussian that peaks at [Fe/H] = −1.59 (metal-poor) and −0.51 (metal-rich) with dispersions of 0.34 and 0.23. T KMM mixture-modeling

Furthermore, We note that the scatter between different Auriga haloes is much smaller than the difference between the MW and M31 GCSs. We conclude that old star particles in the Auriga simulation

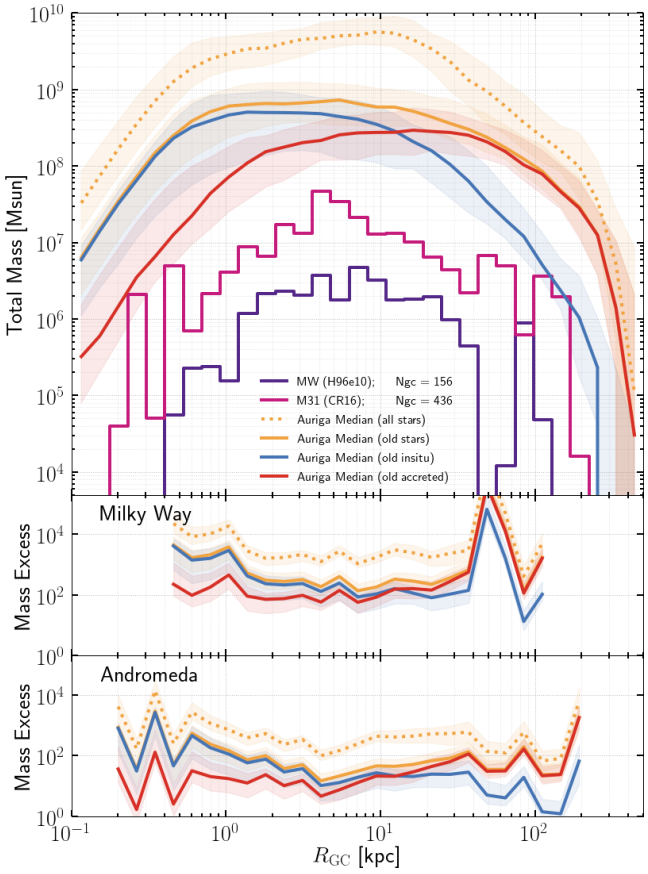

Figure 6. Mass-weighted radial distribution of star particles in the Auriga simulations. We show the median value of all Auriga haloes for all stars (orange dotted) and globular cluster candidates (i.e. stars with age > 10 Gyr; orange solid). The latter sub set is further split up between stars that formed in-situ (blue solid), and those that were accreted (red solid). Shaded regions indicate the 1σ interval. The MW (M31) GCS is shown in purple (magenta). The middle (bottom) panel shows the ratio of the simulated mass to the mass in the MW (M31) GCS.

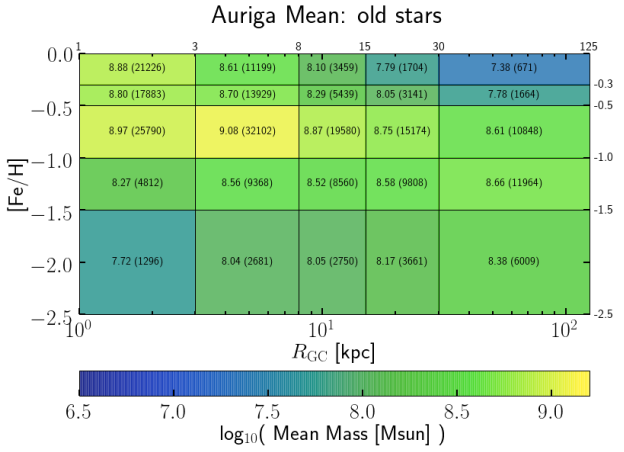

Figure 7. Mass-weighted [Fe/H]-R_{GC} distribution of all Auriga haloes (level 3, 4 and 5). Here we consider the old (> 10 Gyr) stars in all simulations and color-code the **mean value** (of 40 Auriga haloes)

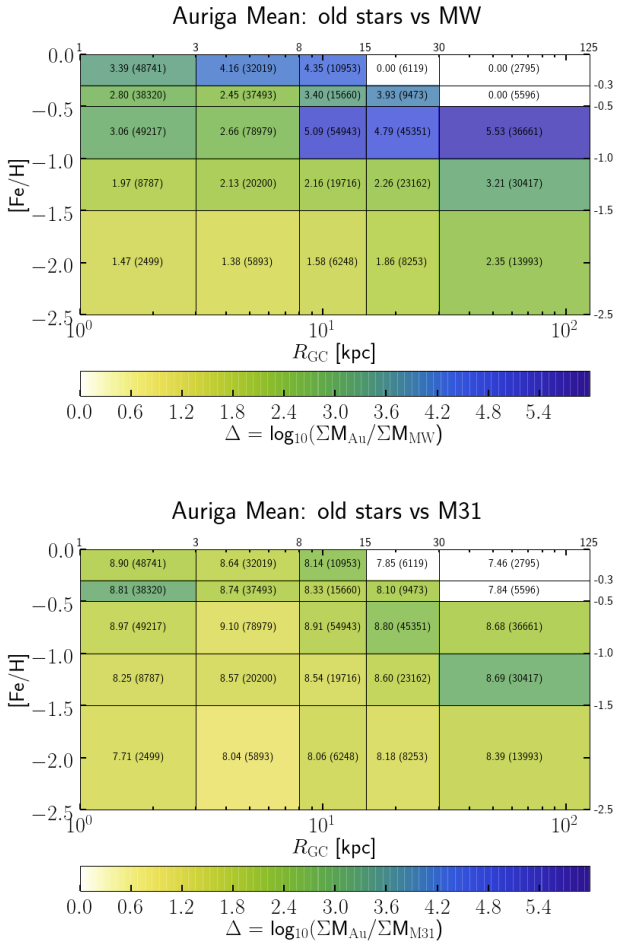

Figure 8. Caption

suite as a whole cannot be consistent with both the Milky Way and the Andromeda globular cluster system.

We observe an increasing trend with increasing metallicity for the Milky Way over the entire range of the data, while the M31 GCS shows this increase only in the range [Fe/H]>-0.5 (although not for the *old accreted* component.

Furthermore we test the null hypothesis that the metallicity distribution of the MW (M31) GCS and the *old*, *old insitu*, and *old accreted* star particles in the Auriga simulations are drawn from the same underlying distribution. We calculate the two-sample Kolmogorov-Smirnov test statistic for all thirty Auriga level 4 haloes and reject the null hypothesis for every halo, for every sub set of star particles at least at the 99.99% confidence level. In addition, the null hypothesis that the metallicity distributions of the MW and M31 GCS are drawn from the same distribution is rejected at the 99.99997% confidence level.

5.2 Radial distribution

Harris: 'Somewhat arbitrarily, I will take the region $r_p > 3$ kpc (containing 75 clusters) as the fiducial Milky Way sample. If we were to view the Milky Way at the same inclination angle to the disk as we see M31, this cutoff in projected distance would correspond roughly to the inner distance limits in the M31 halo sample.'

5.3 Metallicity-radial space

See Figure 2 in Sec. 3.3.

"The fraction of all star formation that occurs in bound stellar clusters (the cluster formation efficiency, hereafter CFE) follows by integration of these local clustering and survival properties over the full density spectrum of the ISM, and hence is set by galaxy-scale physics. We derive the CFE as a function of observable galaxy properties, and find that it increases with the gas surface density" (Kruijssen 2012)

5.4 Age cut

Although the age distribution of M31 Perhaps an age cut of 6 Gyr would would be more appropriate for M31, see Figure 1.

Caldwell & Romanowsky (2016) writes: "there are two broad, well-established differences: (1) the M31 GC system is more populous than the MW system, by a factor of ∼2-3, and (2) it does not exhibit the same obvious bimodality in metallicity (Barmby et al. 2000; Galleti et al. 2009; Caldwell et al. 2011; Cezario et al. 2013). Both of these aspects may be reflections of dramatic differences discovered in these galaxies stellar halos, where the M31 halo appears much more metal-enriched, with massive substructures suggesting a more active satellite accretion history (e.g. McConnachie et al. 2009)"

5.5 From star particles to globular clusters

Star particles are not globular clusters. Many stars do form in clusters, but not all clusters end up gravitationally bound. Star particles in the Auriga simulations represent single-age stellar populations that have formed at the same location within the galaxy. Therefore one could assume a model for the star cluster formation efficiency Γ, which could be used to 'convert' star particles to bound star clusters e.g. Kruijssen (2012). This model relies on the local birth properties of the star particles. However, in our analysis we can retrieve the properties of the star particle in the first snapshot it was recorded, but not the gas properties at times of birth. Therefore we are unable to model the formation of star clusters in more detail.

Furthermore, we compare star particles to present-day globular clusters, thereby ignoring the effects of (dynamical) disruption of globular clusters over nearly a Hubble time. As shown by Pfeffer et al. (2018), a detailed model of the tidal history of star clusters requires a temporal resolution of order mega year. For the Auriga level 4 simulations we have 128 snapshots for the age of the Universe, thus, a far too coarse temporal resolution for meaningful calculations.

Therefore we investigate the over-production of simulated mass in the metallicity and radial bins and use the term 'efficiency' to refer to the combined product of bound cluster formation and globular cluster disruption. In Figure **??** we show the efficiencies that we find

when we compare the simulations to the globular cluster systems of the Milky Way as well as that of Andromeda (M31).

6 SUMMARY AND CONCLUSIONS

ACKNOWLEDGEMENTS

TLRH acknowledges support from the International Max-Planck Research School (IMPRS) on Astrophysics.

Check Auriga boilerplate that we need to acknowledge

RG and VS acknowledge support by the DFG Research Centre SFB-881 'The Milky Way System' through project A1. This work has also been supported by the European Research Council under ERC-StG grant EXAGAL- 308037. Part of the simulations of this paper used the SuperMUC system at the Leibniz Computing Centre, Garching, under the project PR85JE of the Gauss Centre for Supercomputing. This work used the DiRAC Data Centric system at Durham University, operated by the Institute for Computational Cosmology on behalf of the STFC DiRAC HPC Facility 'www.dirac.ac.uk'. This equipment was funded by BIS National E-infrastructure capital grant ST/K00042X/1, STFC capital grant ST/H008519/1 and STFC DiRAC Operations grant ST/K003267/1 and Durham University. DiRAC is part of the UK National E-Infrastructure.

REFERENCES

Ashman K. M., Zepf S. E., 1998, Globular Cluster Systems
Barmby P., Huchra J. P., Brodie J. P., Forbes D. A., Schroder L. L., Grillmair C. J., 2000, AJ, 119, 727
Bica E., Pavani D. B., Bonatto C. J., Lima E. F., 2019, AJ, 157, 12
Brodie J. P., Strader J., 2006, ARA&A, 44, 193
Caldwell N., Romanowsky A. J., 2016, ApJ, 824, 42
Caldwell N., Schiavon R., Morrison H., Rose J. A., Harding P., 2011, AJ, 141, 61
Cezario E., Coelho P. R. T., Alves-Brito A., Forbes D. A., Brodie J. P., 2013, A&A, 549, A60
De Angeli F., Piotto G., Cassisi S., Busso G., Recio-Blanco A., Salaris M., Aparicio A., Rosenberg A., 2005, AJ, 130, 116
Faucher-Giguère C.-A., Lidz A., Zaldarriaga M., Hernquist L., 2009, ApJ, 703, 1416
Galleti S., Federici L., Bellazzini M., Fusi Pecci F., Macrina S., 2004, A&A, 416, 917
Galleti S., Bellazzini M., Buzzoni A., Federici L., Fusi Pecci F., 2009, A&A, 508, 1285
Grand R. J. J., et al., 2017, MNRAS, 467, 179
Harris W. E., 1996, AJ, 112, 1487
Harris W. E., 2001, Globular Cluster Systems. Springer Berlin Heidelberg, p. 223–408, doi:10.1007/3-540-31634-5_2, https://doi.org/10.1007/3-540-31634-5_2
Helmi A., 2008, A&ARv, 15, 145
Huxor A. P., et al., 2014, MNRAS, 442, 2165
Kruijssen J. M. D., 2012, MNRAS, 426, 3008
Mackey A. D., et al., 2019, MNRAS, 484, 1756
Marinacci F., Pakmor R., Springel V., 2014, MNRAS, 437, 1750
McConnachie A. W., et al., 2009, Nature, 461, 66
McLaughlin D. E., van der Marel R. P., 2005, ApJS, 161, 304
Pakmor R., Springel V., 2013, MNRAS, 432, 176
Pakmor R., Marinacci F., Springel V., 2014, ApJ, 783, L20
Pakmor R., Springel V., Bauer A., Mocz P., Munoz D. J., Ohlmann S. T., Schaal K., Zhu C., 2016, MNRAS, 455, 1134
Renaud F., Agertz O., Gieles M., 2017, MNRAS, 465, 3622
Ryu J., Lee M. G., 2018, ApJ, 863, L38
Springel V., 2010, MNRAS, 401, 791
Springel V., Hernquist L., 2003, MNRAS, 339, 289
Springel V., Di Matteo T., Hernquist L., 2005, MNRAS, 361, 776
VandenBerg D. A., Brogaard K., Leaman R., Casagrande L., 2013, ApJ, 775, 134
Veljanoski J., et al., 2014, MNRAS, 442, 2929
Vogelsberger M., Genel S., Sijacki D., Torrey P., Springel V., Hernquist L., 2013, MNRAS, 436, 3031
Wang S., Ma J., Liu J., 2019, arXiv e-prints
Zinn R., 1985, ApJ, 293, 424

APPENDIX A: SCATTER BETWEEN INDIVIDUAL AURIGA HALOES, AND NUMERICAL CONVERGENCE

We check whether the properties of the Auriga globular cluster candidates are well converged between the three different resolution levels used for the Auriga simulations. Here we consider all three Auriga haloes for which simulation runs were performed at all three resolution levels: Au6, Au16, and Au24. Here we can investigate differences between individual haloes.

Figure A1 shows the mass-weighted metallicity distribution, Figure A2 shows the mass-weighted radial distribution, and Figure **??**

This paper has been typeset from a TEX/LATEX file prepared by the author.

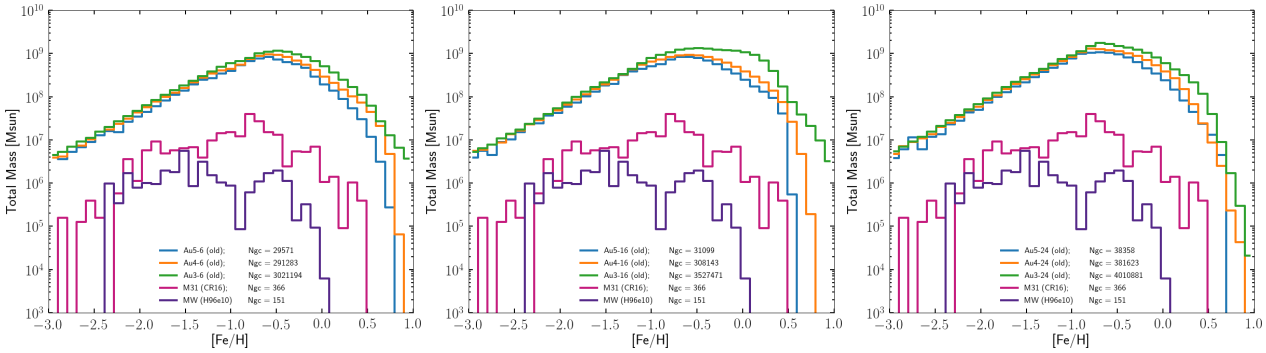

Figure A1. Same as Figure 4, but here the colours indicate resolution level: L3 green, L4 orange, and L5 blue. *Left:* Auriga halo 6. *Mid:* Auriga halo 16. *Right:* Auriga halo 24. For all three haloes we find marginal increases in the mass normalization with increasing resolution level.

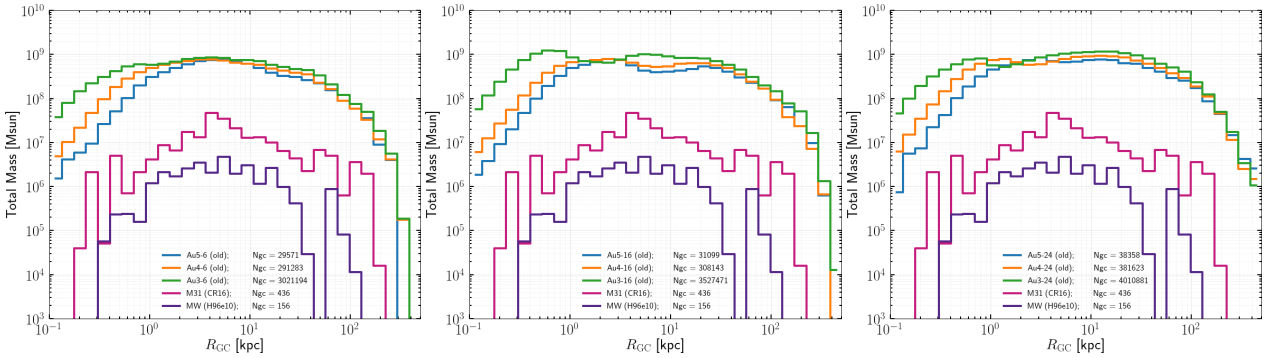

Figure A2. Same as Figure 6, but here the colours indicate resolution level: L3 green, L4 orange, and L5 blue. *Left:* Auriga halo 6. *Mid:* Auriga halo 16. *Right:* Auriga halo 24. For all three haloes we find marginal increases in the mass normalization with increasing resolution level.